relates to the directed dipole of a molecule which one could argue would determine the size and shape of the puncture a molecule made in the dipolar membrane of a neuron. Possibly one could even eliminate the necessity of full penetration of the molecule into the interior of the neuron, and hypothesize that the presence of the molecule on the surface and the consequent disordering of the membrane would be sufficient. The second axis correlates to the first σ electron excitation energy, which one would expect to correlate to Lewis acidity. Whichever one is chosen, it could possibly be sensed by the effect of the molecule on some biochemical pathway which involved electron transfer.

ACKNOWLEDGMENT

The authors thank Dave Kalman, who helped us decipher the CNDO data, Carl Appellof and Jim Koskinen for writing the 3-dimensional model building program, and M. da Koven for moral support.

LITERATURE CITED

(1) Aristotle, "De Anima", book II, Chap. 9, 400 B.C.
(2) T. C. Lecretius, "On the Nature of the Universe", 47 B.C.
(3) H. Zwaardemaker, "Die Psycologie des Geruchs", Englemann, Leipzig, 1895.
(4) H. Hemming, "Der Geruchs", Leipzig, 1912.
(5) E. C. Crocker and L. F. Henderson, *Am. Perfum.*, **227**, 325, 356 (1927).
(6) J. E. Amoore, "Molecular Basis of Odor", C. C Thomas Co., Springfield, Ill., 1970.
(7) G. M. Dyson, *Chem. Ind. (London)*, **1938**, 647 (1938).
(8) R. H. Wright, "The Science of Smell", Basic Books New York, N.Y., 1964.
(9) R. H. Wright and K. M. Michaels, *Ann. N.Y. Acad. Sci.*, **116**, 535 (1964).
(10) S. S. Schiffman, *Science*, **185**, 112 (1974).
(11) L. Guttman, *Psychometrica*, **33**, 469 (1968).
(12) J. T. Davies, "Olfactory Theories" in "Handbook of Sensory Phenomina IV. Chemical Senses 1. Olfaction", L. M. Beidler, Ed., Springer-Verlag, New York, N.Y., 1971.
(13) K. R. Brower and R. Schafer, *J. Chem. Educ.*, **52**, 538 (1975).
(14) D. G. Moulton, "Detection and Recognition of Odor Molecules" in "Gustation and Olfaction", G. Ohloff and A. F. Thomas Ed., Academic Press, New York, N.Y., 1971.
(15) J. A. Pople and D. L. Beverige, "Approximate Molecular Orbital Theory", McGraw, Hill, New York, N.Y., 1970.
(16) "Atlas of Spectral Data and Physical Constants for Organic Compounds, J. G. Grasselli, Ed., C. R. C. Press, Cleveland, Ohio, 1974.
(17) B. R. Kowalski, "Pattern Recognition in Chemical Research", in "Computers in Chemical and Biochemical Research", Vol. 2, C. E. Klopfenstein and C. L. Wilkins, Ed., Academic Press, New York, N.Y., 1974.
(18) B. R. Kowalski and C. F. Bender, *Pattern Recognition*, **8**, 1 (1976).
(19) B. R. Kowalski and C. F. Bender, *J. Am. Chem. Soc.*, **95**, 686 (1973).
(20) J. L. Fasching, D. L. Duewer, and B. R. Kowalski, *Anal. Chem.*, **48**, 2002 (1976).

RECEIVED for review October 26, 1976. Accepted December 20, 1976. This paper was presented at the 172nd National Meeting of the American Chemical Society, San Francisco, Calif., August 1976. This work was supported by the National Science Foundation under grant number MPS 74-00818 A01.

Mercury–Gold Minigrid Optically Transparent Thin-Layer Electrode

Michael L. Meyer,[1] Thomas P. DeAngelis,[2] and William R. Heineman*

Department of Chemistry, University of Cincinnati, Cincinnati, Ohio 45221

An optically transparent thin-layer electrode (OTTLE) with characteristics of mercury has been prepared by electrodepositing a thin film of mercury on a 500-lpi gold minigrid. The negative potential range of this Hg-Au OTTLE was 500 mV greater than that obtained on a Au OTTLE and 200 mV greater than that reported for a Hg-Ni OTTLE. The large hydrogen overvoltage is attributed to the good overvoltage characteristics of the gold substrate, which is quite soluble in mercury, and to the formation of a continuous mercury film rather than droplets. The optical transparency of the gold minigrid (60%) was not measurably diminished by deposition of the mercury film. The extended negative potential range is useful for observing electrode processes with large negative reduction potentials as illustrated by vitamin B_{12} and glyoxylic acid.

Optically transparent electrodes (OTEs) enable spectral monitoring of electrode processes during an electrochemical experiment by virtue of an optical beam passing through the electrode itself (*1–3*, and references therein). Spectroelectrochemistry with OTEs has been used to study the kinetics of homogeneous chemical reactions coupled to electrode processes; obtain UV, visible, and infrared spectra of intermediates and products of electrode reactions; measure $E^{\circ\prime}$ and n values of biological redox components; and observe surface phenomena. In these studies two types of OTEs are commonly employed. The first type of OTE consists of a thin film of a metal (platinum, gold) or a semiconductor (SnO_2, InO_2, carbon) which is coated on a transparent substrate such as glass, quartz, or germanium, depending on the spectral region of interest. The transparency of these electrodes depends on the thinness and the optical properties of the conducting film. A second category of OTE is the minigrid electrode which consists of a metal (gold, nickel, silver, copper) grid with from 100 to 2000 wires per inch (*4*). In this case the transparency is due to the physical holes in the minigrid structure.

Mercury has been used extensively as an electrode material, in part because of its large hydrogen overvoltage which offers a substantially greater negative potential range compared to many other electrode materials such as platinum. Mercury has also proven to be very suitable for the reduction of metal ions to metals which form amalgams. These important properties of mercury have stimulated the development of mercury OTEs. Of particular importance is the extended negative potential range which would make accessible the study of electrode processes obscured by hydrogen evolution on the existing OTEs.

"Mercury" OTEs have been reported for both of the two categories of OTEs described above by electrodepositing a thin mercury coating on a platinum-film OTE (*5*) and on a nickel minigrid OTE (*6*). While both of these electrodes exhibited substantial mercury character including a hydrogen overvoltage increase of 300–600 mV, the influence of dissolved substrate (Pt, Ni), and the formation of mercury droplets rather than a continuous film prevented the attainment of an

[1] Present address, Institute of Forensic Medicine, Toxicology, and Criminalistics, 3159 Eden Ave., Cincinnati, Ohio 45219.
[2] Present address, Corning Glass Works, Corning, N.Y. 14830.

Table I. Variation of Negative Potential Limit with Amount of Mercury Deposited on Gold Minigrid

Concentration of Hg^{2+} deposition solution, mM	Amount of mercury deposited, nmol cm^{-2} [a]	Negative potential limit, V vs. SCE[b]
0	0	−0.50
0.2	2	−0.62
0.6	5	−0.70
2.6	21	−0.84
5.2	42	−0.88
9.6	77	−0.91
satd (~250)	2000	−0.93

[a] Amount deposited per unit area of minigrid assuming exhaustive electrolysis of Hg^{2+}. Cell volume is 30 μL. Macroscopic electrode area is 3.8 cm^2. [b] Potential at which cathodic current exceeds 25 μA (current density, 7 μA cm^{-2}).

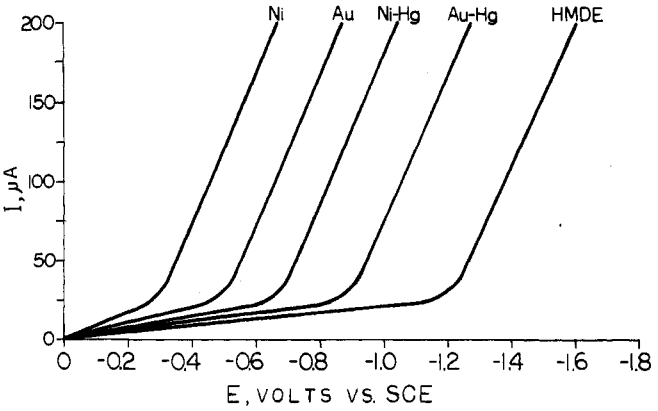

Figure 1. Voltammograms for various electrode materials illustrating respective negative potential limits in 0.1 M HCl, 0.5 M KCl. Scan rate, 5 mV s^{-1}

electrode with the negative potential range of pure mercury. This problem of amalgamation of substrate by the electrodeposited mercury is particularly severe in the case of the platinum-film OTE since the overlying mercury coat must be very thin (ca. <500 Å) in order to retain reasonable optical transparency. Thus, slow contamination of the mercury by substrate amalgamation cannot be countered by deposition of a thick mercury film. Also, coalescence of the droplets into a continuous film by vigorous evolution of hydrogen (*7*) disintegrates the platinum film (*5*).

In a search for improved substrates for mercury OTEs, several transition metals which have extremely low solubility in mercury (iron, $<5 \times 10^{-7}$ wt %; chromium, $<4 \times 10^{-7}$ wt %; vanadium, 4×10^{-6} wt %; and tungsten, $<1 \times 10^{-5}$ wt %) were examined (*8, 9*). The low solubility was expected to minimize the effect of dissolved substrate on the electrode properties of the electrochemically deposited thin mercury film. In all cases mercury film formation was poor. The electrodes effectively retained the electrochemical characteristics of the substrate metals, the hydrogen overvoltage being unaffected by mercury deposition. The poor film formation on these metals suggests that some solubility of substrate in mercury is beneficial in forming a continuous mercury film which adheres well to the substrate. [Recent evidence suggests that formation of organomercurial compounds might be responsible for the adherence of mercury to graphite substrates (*10*).]

Another approach for maximizing the negative potential range involves depositing the mercury film on a substrate which itself exhibits a good negative potential range. The effects of mercury contamination by substrate amalgamation would then be minimized. A metal which exhibits one of the better negative potential ranges is gold (*11*). Although gold is quite soluble in mercury (0.13 wt %), it has served as a substrate for mercury film electrodes in conjunction with a rotating disk electrode (*12*). The solubility of gold in mercury has been used to give smoother mercury films on platinum by gold-plating the platinum before exposure to mercury (*13, 14*). The deposition of a monolayer of mercury on a rotating gold disk electrode has been used for the trace analysis of mercury(II) (*15*). Complex amalgam systems involving gold have been extensively investigated (*16*).

We report here the characterization of a "mercury" OTE consisting of a thin mercury film electrodeposited on a gold minigrid OTE. Although gold is very soluble in mercury, the negative potential range of this Hg-Au OTE is substantially greater than that obtained for OTEs consisting of mercury films on the less soluble platinum and nickel substrates. The electrode was characterized in a thin-layer cell.

EXPERIMENTAL

Apparatus. Optically transparent thin-layer electrodes, OTTLEs, were assembled from microscope slides, Teflon tape spacers, and minigrid electrodes as reported previously (*4, 17*). The transparent electrodes used were 500 lines per inch, 60% transmittant gold and 333 lines per inch, 57% transmittant nickel minigrids (Buckbee Mears Co., St. Paul, Minn.). The OTTLEs were precleaned with a Harrick Plasma Cleaner (Harrick Scientific Co., Ossining, N.Y.). All potential measurements were vs. a saturated calomel electrode. The potentiostat used for electrochemical measurements was of conventional operational amplifier design. System response signals were recorded on a Houston Instrument 2200-5-6 X-Y recorder with time base. A Princeton Applied Research Model 174 polarographic analyzer was used to record cyclic voltammograms at the hanging mercury drop electrode in various supporting electrolytes. The B_{12} optical experiment was performed in a spectrometer consisting of a tungsten lamp source, a Schoeffel GM 100 miniature grating monochromator, and a PMT detector.

Scanning electron micrographs were taken with a JEOL JSM-U3 scanning electron microscope at the Winton Hill Technical Center of the Procter and Gamble Company.

Reagents. The saturated Hg^{2+} solution used for deposition of mercury on the Au OTTLE was saturated $Hg(NO_3)_2 \cdot H_2O$ (ca. 0.25 M), 0.5 M KCl, 0.1 M HCl. The vitamin B_{12} solution was 1 mM vitamin B_{12}, 0.5 M KCl. Glyoxylic acid solution was prepared by a 1:20 dilution of 1.5×10^{-2} M stock glyoxylic acid (Aldrich Chemical Co., Milwaukee, Wis.) in pH 13 buffer, 0.2 M KCl. All other solutions were made with reagent grade chemicals diluted with distilled, deionized water.

Procedure. The following procedure gave a mercury–gold OTTLE with the greatest hydrogen overvoltage. A gold minigrid OTTLE was first placed in the Plasma Cleaner for 5 min. The Plasma Cleaner is a radiofrequency discharge which removes organic material adsorbed on the minigrid and microscope slides. This procedure has been found to minimize the entrapment of air bubbles during solution addition to the OTTLE (*17*). The minigrid was then plated with mercury by electrodeposition in two separate steps. First a solution consisting of saturated $Hg(NO_3)_2$, 0.5 M KCl, 0.1 M HCl was drawn into the cell. A potential of approximately −0.7 V vs. SCE was then applied to the electrode and maintained until the entire electrode turned a dull gray color. Once this color change was completed, the electrode was rinsed with distilled, deionized water. In the second step, a solution consisting of supporting electrolyte (e.g., 0.5 M KCl, 0.1 M HCl) was drawn into the cell and a larger negative potential applied (approximately −1.2 V vs. SCE). This potential was maintained until the electrode color changed from the dull gray to a shiny gray. The completion of this second color change was accompanied by a rapid decrease in the current. The electrode was then ready for use after thorough rinsing with distilled water.

RESULTS AND DISCUSSION

Negative Potential Range. An important objective in the development of a mercury OTE is achievement of the greatest possible negative potential range. The effect on negative potential limit of increasing amounts of mercury deposited on

Table II. Negative Potential Limits on Various Electrodes

Supporting electrolyte	Negative potential limit, V vs. SCE[a]						
	Au OTTLE	New Hg-Au OTTLE	Old Hg-Au OTTLE[b]	Replated Hg-Au OTTLE[c]	Ni OTTLE	Hg-Ni OTTLE	HMDE
0.5 M Na_2SO_4, 0.05 M H_2SO_4	−0.55	−0.95	−0.87	−1.03	−0.38	−0.72	−1.28
0.5 M KNO_3, 0.1 M HNO_3	−0.35	−0.87	−0.75	−0.94	−0.11	−0.75	−1.12
0.5 M KCl, 0.1 M HCl	−0.50	−0.87	−0.83	−0.94	−0.30	−0.66	−1.21
0.5 M Na_2SO_4	−1.09	−1.56	−1.47	−1.56	−0.70	−1.28	−1.83
0.5 M KNO_3	−1.14	−1.50	−1.41	−1.52	−0.81	−1.28	−2.18
0.5 M KCl	−1.15	−1.60	−1.34	−1.59	−0.86	−1.18	−1.98
pH 7.0 phosphate buffer	−1.02	−1.42	−1.29	−1.40	−0.61	−1.02	−1.66

[a] Potential at which cathodic current exceeds 7 μA cm^{-2}. [b] Measurements made 3 days after mercury plating. [c] Measurements made immediately after replating an old electrode.

a 500-lpi gold minigrid is shown in Table I. The experiment consisted of first depositing a given amount of mercury on the gold minigrid by exhaustive reduction of the Hg^{2+} in the thin layer by the procedure given in the Experimental section. The cell was then rinsed and a negative potential scan recorded on a solution of 0.1 M HCl, 0.5 M KCl. Table I shows the potential at which hydrogen commenced to evolve (current density exceeded 7 $\mu A/cm^2$) as a function of the amount of mercury deposited on the minigrid. A new minigrid was used for each experiment and the amount of mercury deposited was determined by the concentration of mercuric solution. As the data show, the potential for hydrogen evolution shifted negatively as increasing amounts of mercury were deposited. A negative shift of 500 mV was achieved with a saturated mercuric solution. Additional amounts of mercury deposited on the same minigrid gave no further improvement. This behavior is analogous to results of mercury deposition on platinum (*5*) and nickel (*6*) substrates where the hydrogen overvoltage could be increased up to 300 to 600 mV beyond that on the substrate metal by increasing the thickness of the electrodeposited mercury film.

A single deposition of saturated mercuric solution gave the electrode with the greatest negative potential range. This amount of mercury deposited on the 500-lpi minigrid corresponds to a mercury film thickness of 4500 Å, assuming a uniform coverage on the minigrid wires (*5*). Interestingly, multiple depositions of mercury from a solution of lower concentration gave no additional overvoltage beyond that achieved with the initial deposition. The best electrode was achieved by a single deposition of a saturated Hg^{2+} solution. This is different from the results with nickel minigrids in which the best electrode was prepared by multiple depositions from mercuric solutions of lower concentration (*6*).

Figure 1 shows a comparison of voltammograms of 0.1 M HCl, 0.5 M KCl solution recorded on gold and nickel minigrids, mercury-coated gold and nickel minigrids, and a hanging mercury drop electrode. Although gold is considerably more soluble in mercury (0.13 wt %) than is nickel (2×10^{-6} wt %), mercury-coated gold minigrids exhibit a substantially greater negative potential range than the mercury-coated nickel minigrid. This is due in part to the greater hydrogen overvoltage on gold compared to nickel. As shown in Figure 1, the hydrogen overvoltage on pure gold is ca. 200 mV greater than on pure nickel. This same overvoltage increment extends to the mercury-coated substrates. Evidently the effect on overvoltage of the greater solubility of gold in mercury, which would diminish the purity of the mercury film, is offset by the better hydrogen overvoltage properties of gold compared to nickel. A second consideration is smoothness of the mercury film. Unfortunately, the electrodeposition of mercury on substrates with low solubility in mercury exhibits a distinct tendency to form mercury droplets rather than a smooth, continuous film. This applies to both nickel (*6*) and platinum (*5*) as well as to the commonly used carbons and graphites (*18–20*) and a variety of other metals (*9*). Consequently, the hydrogen overvoltage is a composite of the overvoltage on mercury droplets and exposed substrate. As discussed below, a relatively even film of mercury is formed on the gold minigrid. No droplets of mercury were formed on any Hg-Au minigrid examined. Evidently, the propensity of Au for amalgamation precludes the formation of mercury droplets, causing a smooth film with little exposed substrate. This also explains the low residual current for the Hg-Au minigrid which is substantially lower than on the Hg-Ni minigrid and approaches the low residual current on pure mercury (*21*).

The hydrogen overvoltage of a freshly coated gold minigrid shifts only about 50 mV positively during the first 6–8 hours after deposition. This slow shift continues to 100–200 mV after 24 h. The original overpotential can be regenerated by repeating the mercury deposition procedure. The electrochemical behavior of a freshly replated old electrode is indistinguishable from a new electrode with the first mercury coat. Replating can be repeated 3–4 times before amalgamation deteriorates the underlying gold minigrid to the extent that it falls apart.

Table II shows the negative potential limits obtained with several electrodes on a variety of solutions of various pH's. Since thin-layer electrochemical techniques have been shown to be useful for the study of biological redox components (*17, 22*), some of these solutions were investigated because of their biological utility.

Microscopic Observation. The sheets of gold minigrid from which electrodes are cut have distinguishable sides as a result of the electrodeposition procedure by which they are fabricated. One side is a shiny metallic yellow, the other is a dull yellow. Figures 2A and 2B show scanning electron microscope photographs of the two sides of a 500-lpi gold minigrid. The dull yellow side shown in Figure 2A is characterized by a distinctly crystalline surface texture. By comparison, the shiny yellow side in Figure 2B is smooth, showing the outline of the template upon which the minigrid was deposited.

During the preparation of a Hg-Au minigrid by the procedure outlined in the Experimental section, the minigrid underwent distinct color changes from the original gold to dull gray (during the first step of the procedure) and then to shiny gray (during the second step). Figure 2C is a scanning electron micrograph of an electrode (shiny side) in the intermediate dull gray state. The electrode is covered with small crystals. Although the potential was stepped to a value sufficiently negative for reduction of Hg^{2+} to Hg^0, the potential of the minigrid in fact "scans to the applied potential" as a result of the large resistance in the thin layer. The formation of Hg(I)

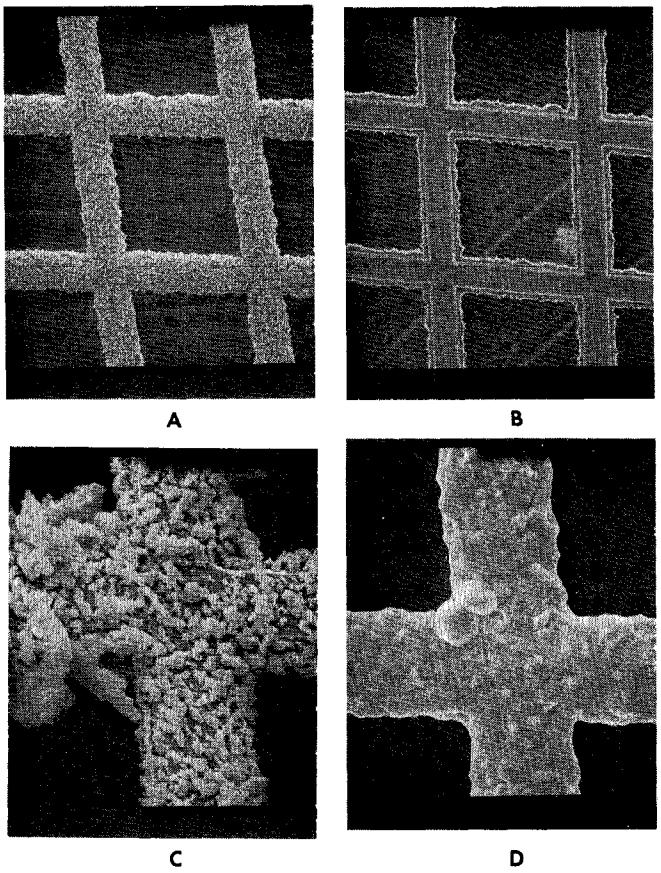

Figure 2. Scanning electron micrographs

(A) Gold minigrid, dull side; magnification 1000×. (B) Gold minigrid, shiny side; magnification 1000×. (C) Mercury–gold minigrid showing crystal formation; magnification 3000×. (D) Freshly plated mercury–gold minigrid; magnification 3000×

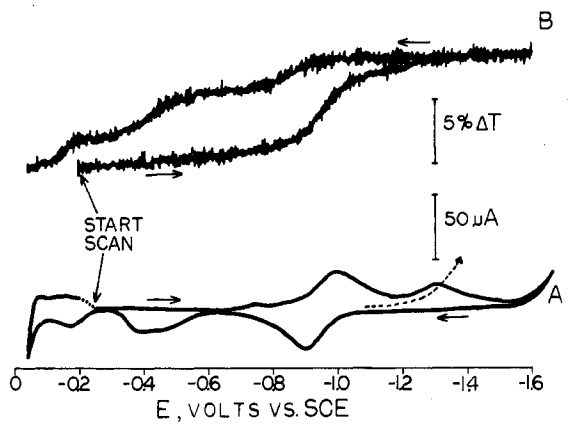

Figure 3. Current–potential and transmittance–potential curves of vitamin B_{12} in Hg-Au OTTLE

(A) Cyclic voltammogram of 1 mM vitamin B_{12}, 0.5 M KCl at the mercury–gold electrode; scan rate, 5 mV s^{-1}. (B) Change in transmittance at 520 nm corresponding to various oxidation states of Co in vitamin B_{12}

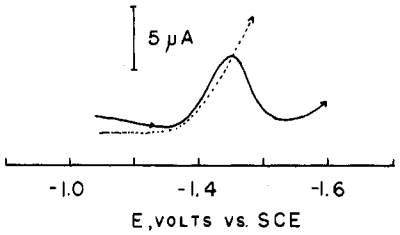

Figure 4. Voltammogram of glyoxylic acid in pH 13 buffer. Scan rate, 2 mV s^{-1}. Hg-Au OTTLE

during this "scan" results in precipitation of what is probably Hg_2Cl_2 ($S = 2 \times 10^{-4}$ g/100 ml at 25 °C), since its solubility is considerably less than that of $HgCl_2$ ($S = 6.9$ g/100 ml at 25 °C) with which the solution was saturated. The dull gray color transforms to the final shiny gray as the crystals are reduced to elemental mercury during the second step in the procedure. The elemental mercury forms a smooth coating on the minigrid as shown in Figure 2D. Since Figure 2D is a photograph of the dull (rough) side of the minigrid, the smoothing can be seen by comparison with Figure 2A. As would be expected if the crystals in Figure 2C are Hg_2Cl_2, no intermediate dull gray step is visually observed if lower concentrations of Hg^{2+} are used for the plating solution (the solubility of Hg_2Cl_2 is not exceeded) or Cl^- is eliminated from the media (deposition solution is $Hg(NO_3)_2$ in 0.1 M HNO_3, 0.5 M KNO_3). In these two cases, the color changes directly from yellow to shiny gray during deposition. We have found that the best Hg-Au electrode is made by the two-step deposition method as outlined above. Deposition of Hg^{2+} from a $Hg(NO_3)_2$ solution causes formation of large mercury droplets along the top and bottom edge of the minigrid due to diffusion from the solution adjacent to the minigrid.

Optical Transparency. The optical transparency of the gold minigrid was not measurably diminished by depositing the mercury coating. Since the optical transparency of minigrid electrodes is a result of holes in the electrode, substantially thicker mercury films can be deposited on minigrids with a negligible decrease in transparency as compared to mercury deposition on a vapor-deposited thin metal film such as platinum. The mercury deposits reported here were ca. 4500-Å thick with retention of the 60% transparency of the unplated gold minigrid compared to a ca. 300-Å thick mercury film on a ca. 400-Å thick platinum substrate for an electrode transparency of ca. 20% for the Hg-Pt OTE (*5*). The commercial availability of gold minigrids in a variety of meshes obviates the necessity for vapor depositing thin metal-film substrates for the mercury. Since the transparency of the electrode is a result of holes, the electrode is useable throughout the entire UV–visible–IR range. A disadvantage of the minigrid is the inability to optically observe interfacial phenomena such as adsorption or to monitor deposition of metals into the Hg as has been demonstrated on the Hg-Pt OTE (*5*).

Vitamin B_{12}. A good example of the usefulness of the Hg-Au minigrid for spectroelectrochemical studies is vitamin B_{12}. Figure 3A shows a vitamin B_{12} cyclic voltammogram which was obtained on a Hg-Au minigrid in a thin-layer cell. The dotted line shows the negative potential limit caused by hydrogen evolution on the Hg-Ni minigrid which obscures the reduction wave at −1.3 V (*23*). The absorbance change at 520 nm which accompanies the conversion of vitamin B_{12} between Co^{III}, Co^{II}, and Co^{I} during the voltammogram is shown in Figure 3B. The extended negative range using the Hg-Au minigrid has also permitted a thorough evaluation of the spectroelectrochemical behavior of 5′-deoxyadenosylcobalamin, which was not previously possible because of the highly negative reduction potential of the cobalamin coenzyme (*24*).

Glyoxylic Acid. Although the main emphasis of this report involves the Hg-Au minigrid as an OTE, the extended negative potential range can also be useful for electroanalysis. An example is glyoxylic acid which, as a result of its quite negative reduction potential, is usually analyzed at a mercury electrode (*25*). As shown in Figure 4, we have been able to observe this reduction in a pH 13 buffer with the Hg-Au OTTLE. The dotted line represents the negative potential limit of the

Hg-Ni OTTLE at this pH, showing that the glyoxylic acid wave is obscured by hydrogen evolution at this electrode. As a result of the extended negative range, glyoxylic acid could be analyzed by thin-layer coulometry and by thin-layer differential pulse voltammetry in the Hg-Au OTTLE (*26, 27*).

Reduction of Metals. The utility of the Hg-Au minigrid for the reduction of metal ions to the elemental form is limited by the tendency of the gold which is dissolved in the mercury film to form intermetallic compounds with other metals (Cd, Mn, Sn, Zn) deposited in the mercury (*28*). For example, lead, which does not form an intermetallic compound with gold, gave a well-behaved, reversible cyclic voltammogram at the Hg-Au minigrid. By contrast, cadmium gave a good reduction wave, but the oxidation wave for Cd^0 was absent due to the formation of a Cd-Au intermetallic compound.

ACKNOWLEDGMENT

The authors gratefully acknowledge J. P. Haberman and D. A. Hudson, The Procter and Gamble Company, Cincinnati, Ohio, for the scanning electron microscope photographs.

LITERATURE CITED

(1) T. Kuwana and W. R. Heineman, *Acct. Chem. Res.*, **9**, 241 (1976).
(2) N. Winograd and T. Kuwana, in "Electroanalytical Chemistry", Vol. 7, A. J. Bard, Ed., Marcel Dekker, New York, N.Y., 1974.
(3) T. Kuwana, *Ber. Bunsenges. Phys. Chem.*, **77**, 858 (1973).
(4) R. W. Murray, W. R. Heineman, and G. W. O'Dom, *Anal. Chem.*, **39**, 1666 (1967).
(5) W. R. Heineman and T. Kuwana, *Anal. Chem.*, **43**, 1075 (1971); **44**, 1972 (1972).
(6) W. R. Heineman, T. P. DeAngelis, and J. F. Goelz, *Anal. Chem.*, **47**, 1364 (1975).
(7) A. M. Hartley, A. G. Hiebert, and J. A. Cox, *J. Electroanal. Chem.*, **17**, 81 (1968).
(8) A. F. Trotman-Dickenson, Ed., "Comprehensive Inorganic Chemistry", Vol. 3, Pergamon Press, London, 1973, pp 283–285.
(9) T. P. DeAngelis, Fellowship Report to the Electrochemical Society, *J. Electrochem. Soc.*, **123**, 186C (1976).
(10) R. G. Clem, *Anal. Chem.*, **47**, 1778 (1975).
(11) R. N. Adams, "Electrochemistry at Solid Electrodes", Marcel Dekker, New York, N.Y., 1969, pp 23–24.
(12) B. Miller and S. Bruckenstein, *Anal. Chem.*, **46**, 2026 (1974).
(13) G. Mamantov, P. Papoff, and P. Delahay, *J. Am. Chem. Soc.*, **79**, 4034 (1957).
(14) H. Gerischer, *Z. Phys. Chem. (Leipzig)*, **202**, 302 (1953).
(15) R. W. Andrews, J. H. Larochelle, and D. C. Johnson, *Anal. Chem.*, **48**, 212 (1976).
(16) Z. Galus, *CRC Crit. Rev. Anal. Chem.*, **4**, 359 (1975).
(17) W. R. Heineman, B. J. Norris, and J. F. Goelz, *Anal. Chem.*, **47**, 79 (1975).
(18) M. Stulikova, *J. Electroanal. Chem.*, **48**, 33 (1973).
(19) R. G. Clem, G. Litton, and L. D. Ornelas, *Anal. Chem.*, **45**, 1306 (1973).
(20) G. E. Batley and T. M. Florence, *J. Electroanal. Chem.*, **55**, 23 (1974).
(21) M. L. Meyer, M.S. Thesis, University of Cincinnati, Cincinnati, Ohio, 1976.
(22) B. J. Norris, M. L. Meckstroth, and W. R. Heineman, *Anal. Chem.*, **48**, 630 (1976).
(23) T. M. Kenyhercz, T. P. DeAngelis, B. J. Norris, W. R. Heineman, and H. B. Mark, Jr., *J. Am. Chem. Soc.*, **98**, 2469 (1976).
(24) H. B. Mark, Jr., T. M. Kenyhercz, and P. T. Kissinger, *ACS Symposium Series*, in press.
(25) V. S. Bezuglyi, V. N. Dmitrieva, T. S. Tarasyuk, and N. A. Izmailov, *J. Gen. Chem. USSR*, **30**, 2396 (1960).
(26) T. P. DeAngelis and W. R. Heineman, *Anal. Chem.*, **48**, 2262 (1976).
(27) T. P. DeAngelis and W. R. Heineman, unpublished results.
(28) E. Barendrecht in "Electroanalytical Chemistry", Vol. 2, A. J. Bard, Ed., Marcel Dekker, New York, N.Y., 1967.

RECEIVED May 17, 1976. Accepted January 5, 1977. The authors gratefully acknowledge financial support provided by National Science Foundation Grant GP-41981X. T.P.D. acknowledges summer support by a J. W. Richards Summer Fellowship (The Electrochemical Society) and the Procter and Gamble Company, Cincinnati, Ohio, for financial support through a Procter and Gamble fellowship.

Theory of Error in Factor Analysis

Edmund R. Malinowski

Department of Chemistry and Chemical Engineering, Stevens Institute of Technology, Hoboken, N.J. 07030

A theory of error for abstract factor analysis (AFA) is developed. It is shown that the resulting eigenvalues can be grouped into two sets: a primary set which contains the true factors together with a mixture of error and a secondary set which consists of pure error. Removal of the secondary set from the AFA scheme leads to data improvement. Three types of errors are shown to exist: RE, real error; XE, extracted error; and IE, imbedded error. These errors are related in a pythagorean sense and can be calculated from a knowledge of the secondary eigenvalues, the size of the data matrix, and the number of factors involved. Mathematical models are used to illustrate and verify various facets of the theory.

Factor analysis (FA) is a mathematical technique for solving multidimensional problems of a certain type. Although FA was developed originally to solve psychological and sociological problems (*1*), it is rapidly gaining importance in various fields of chemistry such as gas–liquid chromatography (*2–4*), spectrophotometry (*5–7*), nuclear magnetic resonance (*8, 9*), mass spectroscopy (*10–13*), and drug activity (*14*). This surge in applications was promulgated chiefly by the sudden availability of digital computers required to carry out the tedious calculations as well as an increased awareness of the methodology.

There presently exists a cautious reluctance by the chemical community to become overly excited about FA. Part of this reluctance is due to the fact that deduction of the number of factors operative in a data matrix, the first step in FA, has not been a clear-cut and straightforward procedure.

If the data contained no experimental error, deducing the exact number of factors would present no problem to the analyst. Up to the present time, no method has been devised to determine whether or not a data matrix is truly factor analyzable. By investigating the factor space of the experimental error in relation to the true factor space of the data, for the first time since the conception of factor analysis, we have been able to achieve a partial answer to this problem. The details of our deductive reasoning will be presented in two parts. The first part, presented here, describes the underlying theory. The second part, which is presented in the accompanying paper, provides an interpretation of some of the results of the theory together with applications to real chemical problems.

A Synopsis of Abstract Factor Analysis. Factor analysis (FA) is a mathematical technique which attempts to express a data point as a sum of product functions. A perfectly pure data point d^*_{ik} is a point which contains no experimental error and is perfectly factor analyzable in n space. Such a point can be expressed as a linear sum of n product terms, called factors. Each factor is comprised of a product of cofactors. That is: